JVI Journals.ASM.org

Interactions of the Vaccinia Virus A19 Protein

P. S. Satheshkumar,[a]* L. Renee Olano,[b] Carl H. Hammer,[b] Ming Zhao,[b] Bernard Moss[a]

Laboratory of Viral Diseases, National Institute of Allergy and Infectious Diseases, National Institutes of Health, Bethesda, Maryland, USA[a]; Research Technologies Section, Research Technologies Branch, National Institute of Allergy and Infectious Diseases, National Institutes of Health, Rockville, Maryland, USA[b]

The A19 protein of vaccinia virus (VACV) is conserved among chordopoxviruses, expressed late in infection, packaged in the virus core, and required for a late step in morphogenesis. Multiple-sequence alignments of A19 homologs indicated conservation of a series of lysines and arginines, which could represent a nuclear localization or nucleic acid binding motif, and a pair of CXXC motifs that suggested a zinc finger or redox active sites. The importance of the CXXC motif was confirmed by cysteine-to-serine substitutions, which rendered the altered protein unable to *trans*-complement infectivity of a null mutant. Nevertheless, the cysteines were not required for function of the poxvirus-specific redox pathway. Epitope-tagged A19 proteins were detected in the nucleus and cytoplasm in both infected and uninfected cells, but this distribution was unaffected by alanine substitutions of the arginine residues, which only partially reduced the ability of the mutated protein to *trans*-complement infectivity. Viral proteins specifically associated with affinity-purified A19 were identified by mass spectrometry as components of the transcription complex, including RNA polymerase subunits, RAP94 (RNA polymerase-associated protein 94), early transcription factors, capping enzyme, and nucleoside triphosphate phosphohydrolase I, and two core proteins required for morphogenesis. Further studies suggested that the interaction of A19 with the RNA polymerase did not require RAP94 or other intermediate or late viral proteins but was reduced by mutation of cysteines in the putative zinc finger domain. Although A19 was not required for incorporation of the transcription complex in virus particles, the transcriptional activity of A19-deficient virus particles was severely reduced.

Morphogenesis of the *Poxviridae* occurs within specialized factory regions of the cytoplasm. This process has been studied most intensively for vaccinia virus (VACV), the prototypic member of the family (1). In the accompanying paper (2), we show that the VACV A19 protein is required for the transition of spherical immature virions (IVs) to barrel-shaped infectious mature virions (MVs). In the absence of the A19 protein, spherical, electron-dense, noninfectious particles accumulate. Arrest at a similar stage occurs with several other conditional lethal VACV mutants under nonpermissive conditions, although the proteins affected have a variety of roles. In some cases, the defective virions lack DNA as occurs with mutants of A32 (3), I6 (4), A22 (5), and G5 (6), whereas in other examples, genomic DNA is present. With some mutants, there are processing defects due to repression of the I7 proteinase (7–9) or possibly by the putative G1 proteinase (10, 11). A similar morphogenesis block also occurs when core-associated early transcription factor subunits A7 (12) and D6 (13) are repressed, suggesting that they also have a structural function. For some core proteins, such as A3 (14) and A12 (15), no precise function is known other than their virion location. Thus, we are unable to predict a specific role for A19 based solely on the stage at which it is required for morphogenesis.

We have taken several approaches to learn more about possible roles of the A19 protein. Sequence alignments indicated the presence of two domains that are conserved in all chordopoxvirus A19 homologs. One is a CXXC . . . . . CXXC motif that could be part of a zinc finger (16) or redox active site (17); the other is a sequence enriched in lysines and arginines that could serve as a nuclear localization signal (NLS) (18), which may overlap a DNA or RNA binding domain (19). We investigated the importance of these two motifs by making point mutations and carrying out complementation and additional studies. A second approach was to identify interacting proteins that might provide a clue to function. A previous yeast two-hybrid screen had detected an interaction between the A19 and A12 proteins (20). By employing an affinity tag attached to A19, we were able to confirm the interaction with A12 and discovered additional interactions with a complex containing RNA polymerase, early transcription factors, and other enzymes involved in mRNA synthesis. Although A19 was not required for the packaging of these proteins, the defective particles were impaired in their ability to synthesize RNA.

MATERIALS AND METHODS

Cells and viruses. HeLa and BS-C-1 cells were cultured in Dulbecco's minimal essential medium (DMEM) and Earle's minimal essential medium (EMEM), respectively, both supplemented with 10% fetal bovine serum, 100 units of penicillin per ml, and 100 μg of streptomycin per ml (Quality Biologicals, Gaithersburg, MD). The recombinant viruses vT7LacOI (21), vFS-A19 (2), vFS-A19i (2), vRAP94i (22), vE10i (23), vL3i (24), v3XFlag-H4 (25), vA7-3XFlag (25), and vD6-3XFlag (25) have been described previously (Table 1).

Construction of recombinant viruses. Several new recombinant viruses were constructed in the present study (Table 1). VACV strain Western Reserve (WR) containing A19 with the influenza virus hemagglutinin (HA) epitope tag at the N terminus (vHA-A19) was constructed by recombination with DNA containing the tag modified A19 open reading

Received 9 May 2013 Accepted 18 July 2013
Published ahead of print 24 July 2013
Address correspondence to Bernard Moss, bmoss@nih.gov.
* Present address: P. S. Satheshkumar, Centers for Disease Control and Prevention, Division of High Consequence Pathogens and Pathology, Poxvirus and Rabies Branch, Atlanta, Georgia, USA.

doi:10.1128/JVI.01261-13

TABLE 1 Recombinant VACV used in this study

VACV	Description	Reference
Viruses with FLAG, FLAG-streptavidin (FS), or HA epitope-tagged proteins		
vFS-A19	FS at the N terminus of A19 protein	2
vHA-19	HA at the N terminus of A19	This study
v3X-Flag-H4	3×FLAG at the N terminus of RAP94 (H4)	25
vA7-3X-Flag	3×FLAG at the C terminus of A7 transcription factor	25
vD6-3X FLAG	3×FLAG at the C terminus of D6 transcription factor	25
vFS-H7	FS at the N terminus of H7	This study
vFS-A11	FS at the N terminus of A11	This study
v3XFlag-H4/HA-A19	3×FLAG at the N terminus of RAP94 (H4) and HA at the N terminus of A19	This study
vA7-3XFlag/HA-A19	3×FLAG at the C terminus of A7 and HA at the N terminus of A19	This study
vD6-3XFlag/HA-A19	3×FLAG at the C terminus of D6 and HA at the N terminus of A19	This study
Viruses with inducible protein with or without epitope tag		
vT7LacOI	Parent for making inducible viruses	21
vFS-A19i	Inducibly expresses A19 with FS at the N terminus	2
vRAP94i	Inducibly expresses RAP94 (H4)	22
vE10i	Inducibly expresses E10 redox protein	23
vL3i	Inducibly expresses L3 core protein	24
vRAP94i-FS-A19	Inducibly expresses RAP94 (H4) and FS at the N terminus of A19	This study

frame (ORF) adjacent to the DsRED ORF and flanked by left and right genome flanking sequences. The same DNA was used to make HA-tagged A19 in several different virus backgrounds, including v3XFlag-H4, vA7-3XFlag, and vD6-3XFlag. In each case, the recombinant virus was clonally purified by repeatedly picking plaques that exhibited red fluorescence.

The inducible virus vRAP94i (22) was modified to express A19 with tandem affinity FLAG- and streptavidin-binding peptide (FS) tags by transfecting the DNA construct described in the accompanying manuscript (2) in cells infected with vRAP94i in the presence of isopropyl-β-D-thiogalactopyranoside (IPTG). vRAP94i-FS-A19 was clonally purified by picking green fluorescent protein (GFP) fluorescent plaques. vFS-H7 was generated by a similar approach using homologous recombination and relevant DNA fragments.

***trans*-Complementation protocol.** BS-C-1 cells were infected with 3 PFU of vFS-A19i virus per cell in the absence of IPTG. To determine the *trans*-complementation ability of A19 mutants, a plasmid expressing either wild-type (WT) or mutant FS-A19 gene under the control of its natural promoter was transfected. For a control, a plasmid that expresses FS-tagged H7 regulated by its natural promoter was used. At 24 h postinfection, cells were harvested, and virus yields were determined by plaque assays in BS-C-1 cells in the presence of IPTG or checked for protein expression by Western blotting with anti-FLAG M2 mouse monoclonal antibody (MAb). The complementation efficiencies of WT and mutants were determined from virus yields.

Confocal microscopy. HeLa cells grown on coverslips were infected with vFS-A19 or vHA-A19 for 18 h. The cells were washed with phosphate-buffered saline (PBS) and fixed with 4% paraformaldehyde in PBS and permeabilized with PBS containing 0.1% Triton X-100. The sample was blocked with 10% fetal bovine serum in PBS, followed by incubation with primary antibodies in serum for 1 h. The cells were washed with PBS and incubated with secondary antibodies conjugated to dyes (Molecular Probes, Eugene, OR) for an additional 1 h. Coverslips were mounted on a glass slide with Prolong Gold (Molecular Probes) and viewed with a confocal microscope.

Antibodies. The FLAG epitope tag was detected using either anti-FLAG M2 MAb or anti-FLAG rabbit polyclonal antibody (Sigma-Aldrich, St. Louis, MO). The influenza virus HA epitope tag was detected with anti-HA.11 mouse MAb or anti-HA.11 PRB-101P rabbit polyclonal antibody (Covance, Denver, PA). Mouse MAb 7D11 (26) and rabbit polyclonal antibody R180 (27) against L1 have been described previously. Rabbit polyclonal antibodies used in this study against A7 (28), A11 (29), D6 (28), H4 (30), J6 (RPO147; gift from S. Shuman), J4 (RPO22; gift from S. Shuman), and F9 (31) have been described. Proteins in Western blots were detected by using anti-mouse or anti-rabbit secondary antibodies conjugated to IRDye 680 or 800 and visualized using a LI-COR Odyssey infrared imager (LI-COR Biosciences, Lincoln, NE).

Protein affinity purification. HeLa cells were infected with 5 PFU per cell of VACV WR, vFS-A19, and vFS-A11 viruses. After 16 h, the cells were harvested and resuspended in lysis buffer (50 mM Tris [pH 7.4], 200 mM NaCl, 1% Triton X-100) containing complete protease inhibitor cocktail tablet (Roche, Indianapolis, IN) for 30 min at 4°C. Lysates were clarified by centrifugation at 10,000 × *g* for 15 min at 4°C and allowed to bind to streptavidin-agarose beads for 4 h at 4°C. Beads were washed four times with lysis buffer followed by elution of bound proteins with lysis buffer containing D-biotin (1 mg/ml). Proteins eluted from streptavidin-agarose beads were resolved in NuPAGE 4 to 12% Bis-Tris gels (Life Technologies) and stained with Coomassie blue dye. Each lane was sliced into 20 equal fractions, cut into small pieces with a surgical knife, and subjected to in-gel tryptic digestion, followed by mass spectrometry (MS). For Western blot analysis, proteins were transferred to nitrocellulose membranes and probed with antibodies.

Mass spectrometry and protein identification. Identification of proteins following SDS-PAGE was performed on reduced and alkylated, trypsin-digested samples prepared by standard mass spectrometry protocols. The supernatant and two washes (5% formic acid in 50% acetonitrile) of the gel digests were pooled and concentrated with a SpeedVac instrument (Labconco, Kansas, MO) to dryness directly in 200-μl polypropylene autosampler vials (Sun Sri, Rockwood, TN). The recovered peptides were resuspended in 5 μl of solvent A (0.1% formic acid, 2% acetonitrile, and 97.9% water). Prior to mass spectrometry analysis, the resuspended peptides were chromatographed directly on a column, without trap cleanup. The bound peptides were separated at 500 nl/min by generating a pressure of 80×10^5 to 120×10^5 Pa, using an AQ C18 reverse-phase medium (3-μm particle size and 200-μm pore size) packed in a pulled tip, nanochromatography column (0.100-mm inner diameter [ID]; 150-mm length) from Precision Capillary Columns, San Clemente, CA. The chromatography was performed in-line with an LTQ-Velos Orbitrap mass spectrometer (ThermoFisher Scientific, West Palm Beach, FL), and the mobile phase consisted of a linear gradient prepared from solvent A and solvent B (0.1% formic acid, 2% water, and 97.9% acetonitrile) at room

temperature. Nano-liquid chromatography coupled to tandem MS (nano-LC-MS/MS) was performed with a ProXeon Easy-nLC II multidimensional liquid chromatograph and temperature-controlled Ion Max nanospray source (ThermoFisher Scientific) in-line with the LTQ-Velos Orbitrap mass spectrometer.

Computer-controlled data-dependent automated switching to MS/MS by Xcalibur 2.1 software was used for data acquisition and provided the peptide sequence information. Data processing and data bank searching were performed with Proteome Discoverer 1.2 (ThermoFisher Scientific) and Mascot software (Matrix Science, Beachwood, OH). The data were searched against a sequence file containing VACV proteins found in the UniprotKB TrEMBL database and human proteins found in UniprotKB Swiss-Prot (November 2011) allowing one missed cleavage and mass tolerances of 10 ppm and 0.8 Da for the precursor and fragment ions, respectively. Carbamidomethylation of cysteine was set as a fixed modification, while oxidation of methionine, deamidation of asparagine and glutamine, and protein N-terminal acetylation were searched as dynamic modifications. The resulting search files were reclustered against the same sequence database for further analysis using ProteoIQ software (PREMIER Biosoft, Palo Alto, CA). Assignments were filtered using the Protein Prophet algorithm as implemented within ProteoIQ, with cutoff filters set at 95% for peptides and 99% for proteins. Protein assignments were considered only if they met both the probability thresholds and 2 spectra per peptide sequence/2 peptides per protein minimums. For this analysis, spectra were counted for cutoffs if there was significant overlap of sequence coverage in the case of missed cleavages, and without consideration of modification state. Rough quantification was performed using a simple spectral count method with normalized spectral abundance factors to remove bias resulting from differences in protein length. Normalization between gel lanes was performed using factors derived from the use of ATI_VACCW, A-type inclusion protein (P24759) as a control protein (1, 1.22, and 1.11 for A11, A19, and VACV WR, respectively).

RNA synthesis by purified virus particles. Transcription by detergent-permeabilized virus particles was performed as previously described (24). A19-deficient ($A19^-$) and A19-containing ($A19^+$) virus particles from BS-C-1 cells that had been infected with vFS-A19i in the absence and presence of IPTG, respectively, were purified by sedimentation through a sucrose cushion followed by sedimentation through a sucrose gradient. Similarly, $L3^-$ and $L3^+$ viruses were purified from cells infected with vL3i-inducible virus. Purified viruses were incubated with transcription buffer containing 50 mM Tris-HCl (pH 8.0), 5 mM dithiothreitol, 10 mM $MgCl_2$, 0.05% Nonidet P-40 (NP-40), 5 mM ATP, 1 mM GTP, 1 mM CTP, and 0.02 mM UTP. The reaction was carried out in the presence of 1 μCi of [α-^{32}P]UTP at 30°C for 1 h. RNA synthesis was determined by trichloroacetic acid precipitation on DE51 ion-exchange paper followed by scintillation counting.

RESULTS

Conserved motifs in the A19L ORF. The A19L ORFs from representative members of each chordopoxvirus genus were compared using the ClustalW program (32) in order to identify conserved protein features that might provide a clue to function. The predicted proteins ranged from 72 to 90 amino acids in length with a calculated mass of 8.3 kDa for VACV A19 (Fig. 1A). Pairwise amino acid identity scores between genera varied from 26 to 58% but were much closer within a genus as indicated by the 92% identity between the orthopoxviruses VACV and variola virus (Fig. 1B). Sequence analysis revealed the conservation of multiple positively charged lysine and arginine residues near the N terminus (Fig. 1A), suggesting a nucleic acid binding motif or NLS (19). Another conserved feature near the C terminus was four cysteine residues (Fig. 1A), part of a predicted CXXC . . . . . CXXC zinc finger domain (16). CXXC motifs can also serve at the active sites of thiol-disulfide oxidoreductases (17), which is of particular relevance, because poxviruses carry genes that encode a novel redox system (33). There were no indications of a signal peptide or transmembrane domain in the A19 protein.

Mutational analysis of the A19 protein. To investigate the significance of the above motifs, we constructed site-directed mutants and analyzed their ability to *trans*-complement infectivity of the A19-inducible null mutant described in the accompanying report (2). The four conserved cysteines were mutated to serine residues either in pairs (C31 and C34) or (C62 and C65) or all four together (C31, C34, C62, and C65). Plasmids containing either the WT ORF or one of the mutated ORFs with the natural A19 promoter were transfected into cells that had been infected with vFS-A19i in the absence of IPTG. Use of the viral promoter ensured that transcription would occur in the viral factory. The complementation efficiency was determined by the yield of progeny virus, which was calculated by plaque titration in BS-C-1 cells in the presence of inducer. Mutation of cysteine pairs resulted in a statistically significant decrease in complementation efficiency compared to the WT, and no complementation occurred when all four conserved cysteines were mutated to serines (Fig. 2A). Western blots confirmed that the amounts of mutant proteins were similar to those of WT proteins and not rapidly degraded because of folding problems (Fig. 2B).

Similarly, we investigated the functional requirement of the putative NLS motif by changing the arginine residues to alanines (18). The mutant exhibited about a 60% reduction in complementation efficiency despite comparable levels of the mutated protein (Fig. 2C and D). However, this decrease did not reach high statistical significance.

Intracellular distribution of A19. VACV genome replication and postreplicative transcription and translation occur within specialized compartments of the cytoplasm that are referred to as "viral factories" (34). The factories are usually located adjacent to the nucleus and can be visualized by staining DNA with 4′,6′-diamidino-2-phenylindole (DAPI). Consistent with the cytoplasmic replication of VACV, few viral proteins, e.g., E3 (35) and F16 (36) have been detected in the nucleus, and these are expressed early after infection. In order to determine the intracellular location of A19, we used a recombinant virus with an FS epitope tag (Table 1), as that does not affect replication (2). However, because epitope tags can perturb localization, we also made a replication-competent recombinant VACV with a HA tag, which is smaller than the FS tag, on A19. The intracellular distribution of A19 in cells infected with vFS-A19 and vHA-19 was determined by confocal microscopy using anti-FLAG and anti-HA antibodies. Antibodies to L1, a viral membrane protein, were used as a control. To rule out nonspecific effects, both mouse and rabbit primary antibodies and the corresponding secondary antibodies were employed to detect A19 and L1 proteins. As expected, L1 was predominantly located in viral factories (Fig. 3A and B). In contrast, A19 was distributed in the nucleus and in cytoplasmic factories (Fig. 3A and B). However, whereas the HA-tagged A19 was uniformly distributed in the nucleus, the FS-tagged protein had a patchy distribution mostly within the nuclear cortex.

Transfection experiments were carried out in uninfected HeLa cells to determine whether nuclear localization was dependent on other viral proteins. As shown in Fig. 3C, FS-A19 was distributed in the nucleus and in the cytoplasm. Moreover, the protein was more uniformly dispersed in the nuclei of uninfected cells compared to infected cells. Surprisingly, mutation of the putative NLS

A

```
VACV  ----------------MDSTNVRSGMKSRKK---------KPKTTVIDDD------DD  33
VARV  ----------------MDSTNACSGMKSRKK---------KPKTTVIDED------D-  33
DPV   ------------------MEDTGGAKRIRKR---------KPKTTIQDND------D-  31
YMTV  ------------------MDDMGGAKR-KKR---------KPKIAIQNNN------D-  30
CRV   ------------------MDAGAKQKRRRKR----------ARTTVEDEATTASGTGR  30
SWPV  -------------------MDTAGSKR-KKR---------KPKTTIKDDD--------  29
ORFV  MSAVKAKAGAKGGSKGGVVDVAAGNKKRRRR---------RVTTVVE---------DG  46
MOCV  ------------------MDVSGAKQRRRKR---------KPRTTVEEPPA-----DS  31
MYXV  ------------------MEDDAGVKRRKKR---------KPKAEVEDD---------  30
SPPV  ------------------MEDSAGNKRKKKR---------KPKTTVQDEE--------  31
FWPV  -----------------MADSTAGAKKRKKRSTSATSTRKEPPTVIPEDE--------  41
                                  . ...             .

VACV  CMTCSACQSKLVKISDITKVSLDYINT-MR----GNTLACAACGSSLKLLNDFAS---  77
VARV  CMTCSVCQSKLVKISDITKVSLDYINT-MR----GNTLACTACGSSLKLLNDFAS---  76
DPV   CVTCSSCYSKLIKVSDITKVSLDLYKVSGK----GNTLSCAACGSELRLLNDFVS---  75
YMTV  CVTCSSCHSKLVKVSDITKISLDELKVAGK----GNVLTCSACGSELRLLSGFVS---  74
CRV   KTTCSLCDSKLLTFSSLSNSSFRKIQPCGGVAGAGTALRCSACNSVLTTLRPTQTPAV  88
SWPV  CMTCSSCYSKLVKMSDITTVSLSQYKVVGK----GNTLSCSACGSELRTLNDFVH---  72
ORFV  DPVCSSCNSRLVSIKDVDRLSTLSLGLACS-----STLSCAACGSALTPLRDLAR---  90
MOCV  CTTCSVCQSRLAFFSDVSKLQASPLRMATPG---PDTLHCAACGSALCPLSEFAR---  78
MYXV  CVTCSSCYSKLVKVSDITKVSLHEYKVAGK----GNTLSCAACGSELRLLNGFVN---  73
SPPV  CMICSSCYSKLVKVSDITKVSLNEYKVGGK----GNILTCSACGSELRMLNGFVN---  74
FWPV  CTTCSICQSKLVMFSGVSKYKLSDYLNTGKVF-TNSNIRCKACGSSLCHLRDLSKS--  88
         ** * *.*     .                    . * **.* *  *
```

B

	VACV	VARV	DPV	YMTV	CRV	SWPV	ORFV	MOCV	MYXV	SPPV	FWPV
Identity	100	92.2	57.7	46.2	26.4	52.6	27.7	38.8	51.3	48.7	29.7
Similarity	100	94.8	70.5	66.7	40.7	65.4	42.6	53.8	64.1	65.4	45.1

FIG 1 ClustalW alignment of A19 chordopoxvirus orthologs. (A) Amino acid sequences of A19 orthologs from each representative genus of *Chordopoxvirinae* were aligned using the ClustalW program. VACV, vaccinia virus Western Reserve; VARV, variola virus Bangladesh; DPV, deerpox virus strain W-1170-84; YMTV, Yaba monkey tumor virus Amano; CRV, crocodilepox virus Zimbabwe; SWPV, swinepox virus Nebraska; ORV, Orf virus OV-SA00; MOCV, molluscum contagiosum virus subtype1; MYXV, myxoma virus Lausanne; SPPV, sheeppox virus strain NISKHI; FWPV, fowlpox virus Iowa. Completely conserved amino acids are denoted by asterisks, and highly conserved amino acids are indicated by dots. Gaps introduced to maximize alignment are indicated by the dashes. The bar above the sequences indicates a sequence of positively charged amino acids. (B) Tabulation of the pairwise percent identity and similarity of A19 sequences between different genera.

motif had no effect on the distribution of FS-A19 (Fig. 3C). Transfection experiments also revealed similar intracellular distributions of the mutant and wild-type FS-A19 proteins regulated by the A19 promoter in infected cells (not shown). These data suggest that the nuclear location may be a function of the relatively small size or other features of the A19 protein rather than the putative NLS.

Lack of effect of cysteine mutations of A19 on the cytoplasmic redox pathway. Poxviruses are unique in carrying genes that encode proteins that comprise a cytoplasmic redox pathway (33). The three proteins involved, E10, A2.5, and G4, each contain a CXXC or CXXXC motif that is required for thiol-disulfide transfer (33). Although the known substrates are membrane proteins involved in virus entry (37), abrogation of the pathway results in a block in morphogenesis (23). Functioning of the redox pathway can be conveniently monitored by the effect on electrophoretic migration of substrate proteins. Both the F9 and L1 proteins attain a more compact shape when their intramolecular disulfide bonds are formed, resulting in more rapid migration by SDS-PAGE. Thus, interference with the redox pathway results in a slow-migrating reduced form of the protein, as shown by repression of the E10 redox protein when cells are infected with the inducible vE10i in the absence of IPTG (Fig. 4). However, when we compared the mobility of F9 in cells infected with vFS-A19i in the presence and absence of IPTG, there was no decrease in the mobility of F9 even though A19 was not detected under the latter conditions (Fig. 4). This result indicates that A19 is not required for function of the cytoplasmic redox system.

A19-interacting proteins. HeLa cells were infected with vFS-A19, and the tagged A19 protein was captured with affinity beads to copurify any associated proteins. We also infected cells with two control viruses to evaluate nonspecific interactions: WT VACV, which has no affinity tag; and vFS-A11, which has the same FS affinity tag as A19. Lysates from cells infected with the three viruses were prepared in the same manner and bound to streptavidin-agarose beads. The bound proteins were eluted with biotin and resolved by SDS-PAGE. The absence of any intense bands in the WT lane was expected, as there was no affinity tag (Fig. 5). Surprisingly, the A11 lane had only one intense band corresponding in size to FS-A11, suggesting no strong, stable interactions (Fig. 5). Inspection of the A19 lane, however, revealed many bands that were unique or greatly enriched (Fig. 5). The intense band near the bottom of the gel corresponds in size to FS-A19. To identify proteins, each lane was cut into 20 equal size gel slices and

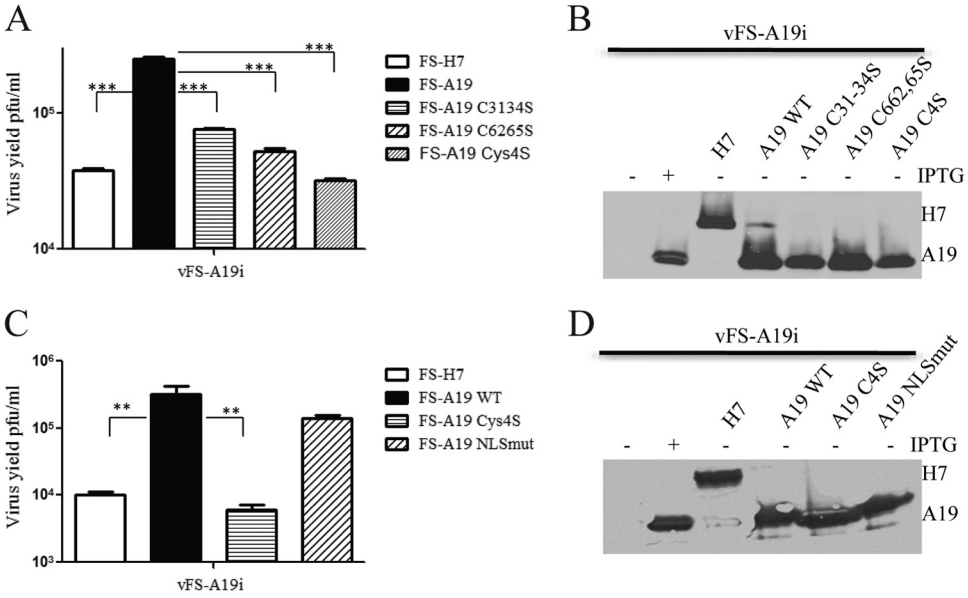

FIG 2 *trans*-Complementation of virus infectivity by A19 mutants. (A) Cysteine mutants. BS-C-1 cells were infected with vFS-A19i in the absence of IPTG and transfected with plasmids expressing wild-type FS-A19 or indicated cysteine mutants. Complementation efficiencies were determined by plaque assay on BS-C-1 cells in the presence of IPTG. C4S is a combination of all four cysteine-to-serine substitutions. Error bars are shown. Statistical significance was determined by one-way analysis of variance (ANOVA) as follows: ***, $P < 0.001$. (B) Western blot analysis. The samples used in panel A were analyzed by Western blotting with anti-FLAG antibodies. (C) NLS mutant. BS-C-1 cells were infected with vFS-A19i in the absence (−) of IPTG and transfected with plasmids expressing H7, wild-type A19, A19 NLS mutant, or C4S mutant. Complementation efficiencies were determined as described above for panel A. Error bars are shown. Statistical significance was determined by one-way ANOVA as follows: **, $P < 0.05$. (D) Western blot analysis of samples described in panel C with anti-FLAG antibodies.

subjected to *in situ* tryptic digestion followed by mass spectrometry. On the basis of comparisons with the two controls, we found selective pulldowns of the following viral proteins by FS-A19: the two large RNA polymerase subunits RPO147 (J6) and RPO132 (A24), the RNA polymerase-associated protein RAP94 (H4), the two early transcription factor (vaccinia virus early transcription factor [VETF]) subunits (E6 and A7), one of the capping enzyme subunits (D1), the nucleoside triphosphate phosphohydrolase NPH I (D11), two core proteins A12 and A3, and a virion protein E2. In contrast, A11 was the only viral protein specifically pulled down by FS-A11 using the criteria of at least 2-fold enrichment over controls. In Table 2, the spectral abundance data were normalized between samples for recovery of the A-type inclusion protein (ATI)-related A25 protein, which was nonspecifically captured in similar amounts from the samples, and within each sample for polypeptide size.

Association of A19 with RAP94 and RNA polymerase. The VACV RNA polymerase, RAP94, capping enzyme, early transcription factor, and NPH I are known to associate with each other to form a complex, but none of these proteins had previously been shown to interact with an unrelated core protein. Western blotting was used to confirm the association of RNA polymerase and RAP94 with A19. Soluble extracts of cells that had been infected with vFS-A19 and vFS-A11 were treated with Benzonase to digest nucleic acids, and the proteins were affinity purified. Antibodies to the large 147-kDa subunit and a small 22-kDa subunit of RNA polymerase were available to probe the Western blot. Positive signals were obtained with the FS-A19 pulldown but not with the control FS-A11 pulldown (Fig. 6A). These results suggested that the holo-RNA polymerase complex, including small and large subunits, was associated in the complex with A19, but that the former were not detected by mass spectrometry because of their size. As predicted from the mass spectrometry data, RAP94 was also detected by Western blotting with the FS-A19 pulldown but not with the FS-A11 pulldown (Fig. 6A). However, we did not detect VETF subunits A7 and D6, which were found by mass spectrometry (Fig. 6A).

The reverse pulldown of A19 with RAP94 was demonstrated by using newly generated recombinant virus v3XFlag-H4/HA-A19, carrying FLAG fused to RAP94 and HA fused to A19. Affinity purification of RAP94 with anti-FLAG antibody-conjugated beads specifically pulled down HA-A19 (Fig. 6B), whereas control virus vHA-A19 without the FLAG tag did not. Using two additional viruses, vA7-3XFlag/HA-A19 and vD6-3XFlag/HA-A19 that had FLAG-tagged A7 and FLAG-tagged D6, respectively, in addition to HA-A19 did not pull down the latter. These data suggested that A19 might be more closely associated with RAP94 than with A7 or D6.

A19 interacts with RNA polymerase independently of RAP94. Based on the above data, A19 could interact directly with RAP94 or RNA polymerase, since the two proteins are tightly associated (30, 38). To resolve this issue, the gene encoding FS-A19 was inserted into the genome of the RAP94 (H4)-inducible virus vRAP94i. Cells were infected with vRAP94i-FS-A19 in the presence and absence of IPTG to prevent synthesis of RAP94 and with a positive-control virus, vFS-A19, and a negative-control virus, vFS-H7. After streptavidin affinity purification of FS-A19 protein, similar amounts of RPO147 and RPO22 were detected in the samples from cells infected with vRAP94i-FS-A19 in the absence and presence of IPTG (Fig. 7A), suggesting that the interaction of A19 with RNA polymerase is not mediated by or dependent on RAP94.

Next, we wanted to determine whether the cysteine mutations

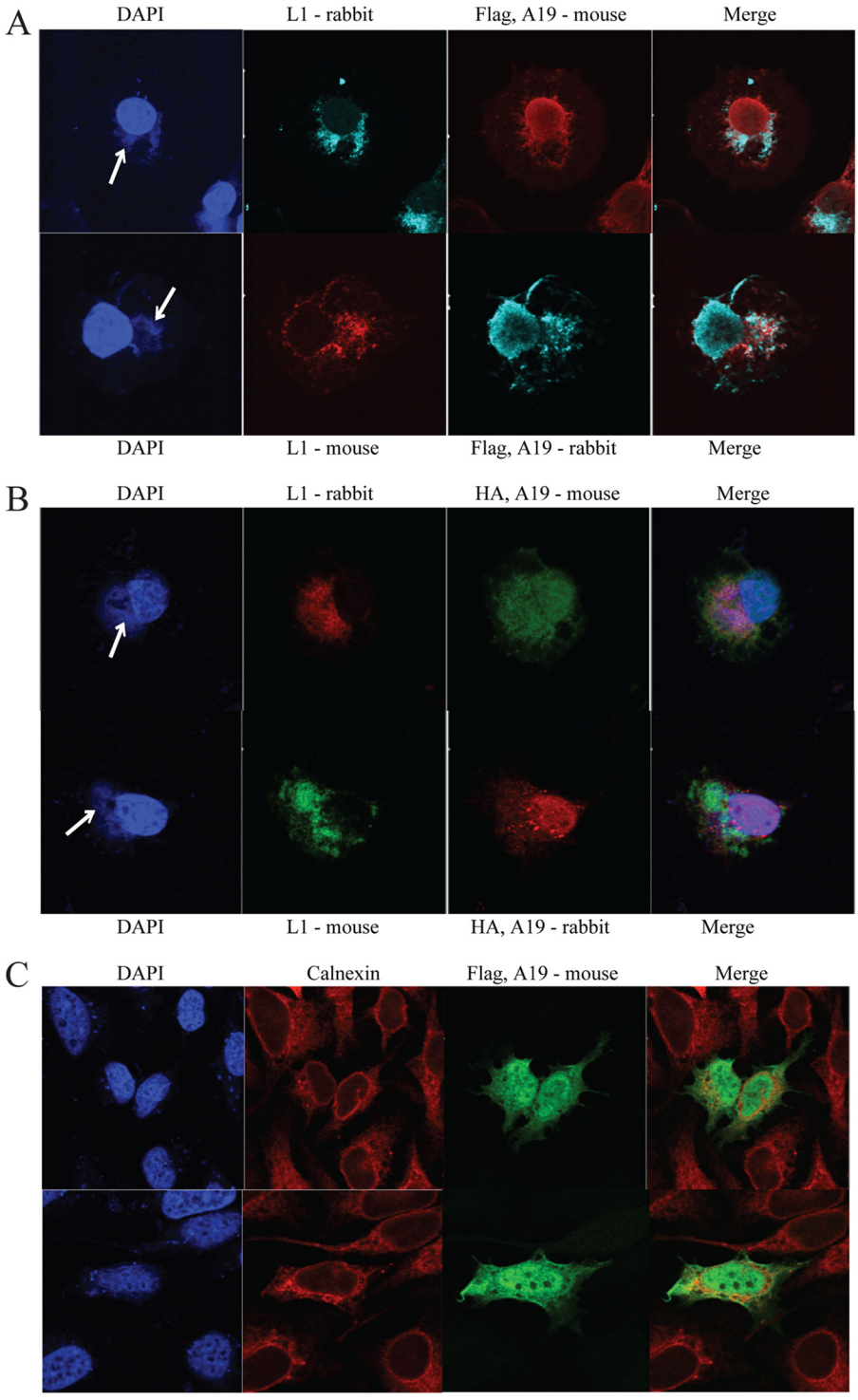

FIG 3 A19 subcellular localization. (A) Detection of the A19 protein in infected cells with FLAG antibody. HeLa cells were infected with vFS-A19 for 24 h, fixed with paraformaldehyde, permeabilized with Triton X-100, and incubated with anti-FLAG mouse MAb M2 and anti-L1 rabbit polyclonal antibody or anti-FLAG rabbit polyclonal antibody and anti-L1 mouse MAb 7D11 followed by the appropriate Alexa Fluor-conjugated secondary antibody. Nuclei and viral factories (white arrows) were detected by staining with DAPI. (B) Detection of A19 in infected cells with HA antibody. HeLa cells were infected with vHA-A19 as described above for panel A and treated as described above for panel A except for the use of anti-HA rather than anti-FLAG mouse MAb and rabbit polyclonal antibody. (C) Detection of A19 in uninfected cells with FLAG antibody. HeLa cells were transfected with cytomegalovirus (CMV) promoter plasmids expressing the wild-type FS-A19 (top panels) or FS-A19 containing NLS mutation (bottom panels). Anti-FLAG M2 MAb antibody was used to detect A19, and anticalnexin rabbit polyclonal antibody was used to label the endoplasmic reticulum.

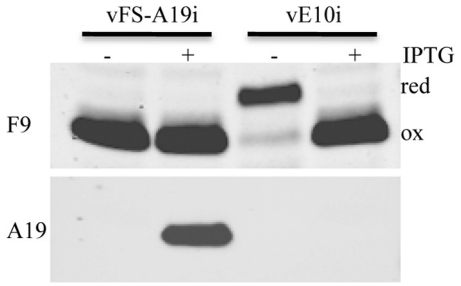

FIG 4 Activity of VACV redox pathway in the absence of A19. BS-C-1 cells were infected with vFS-A19i or vE10i in the presence (+) or absence (−) of IPTG for 18 h. The cells were harvested and lysed by boiling with lithium dodecyl sulfate in sample loading buffer without reducing agent. Proteins were separated by electrophoresis in a 4 to 12% Bis-Tris gel, transferred to a nitrocellulose membrane, and probed with polyclonal antibody to F9 and FLAG MAb. Abbreviations: red, reduced; ox, oxidized.

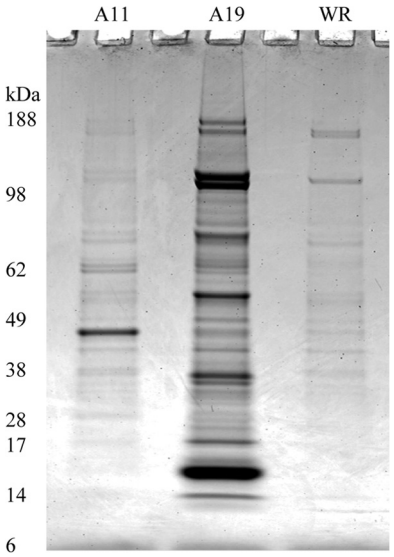

FIG 5 SDS-PAGE of proteins associated with A19. HeLa cells were infected with 5 PFU per cell of VACV Western Reserve (WR), vFS-A19 (A19), or vFS-A11 (A11) for 16 h. The cells were harvested and lysed, and a clarified extract was allowed to bind to streptavidin-agarose beads. After 4 h, the beads were washed and eluted with D-biotin, and the proteins were resolved by SDS-PAGE. The gel was stained with Coomassie brilliant blue. Each gel lane was cut into 20 equal size slices and subjected to *in situ* tryptic digestion followed by mass spectrometry. The positions of molecular mass markers (in kilodaltons) are indicated to the left of the gel.

of the putative zinc finger domain, which prevent complementation of infectivity by A19, would impair association with RNA polymerase. The strategy was to infect cells with vFS-A19i in the absence of IPTG to prevent endogenous A19 expression and to transfect plasmids that express the epitope-tagged WT A19 or combined C4S (C31S, C34S, C62S, and C65S) mutant A19. Proteins were affinity purified with streptavidin-agarose and analyzed by Western blotting. Although expression of FS-A19 was severely repressed in untransfected cells, small amounts were detected in the absence of IPTG, and consequently, the streptavidin beads captured small amounts of RPO147 and a trace of RAP94 (Fig. 7B, left). However, RPO147 and RAP94 were increased when the FS-A19 plasmid was transfected into cells infected with vFS-A19i in the absence of IPTG, correlating with the increased amount of FS-A19 (Fig. 7B, left). Although the FS-A19 with cysteine mutations was expressed to a level comparable to that of the WT protein, less RPO147 and RAP94 were detected (Fig. 7B, left). These data suggested that the A19 cysteine mutant was impaired in its ability to interact with RNA polymerase.

Additional experiments were carried out with a dual purpose. First, to investigate whether additional postreplicative proteins were needed for the interaction between A19 and RNA polymerase and second to confirm the difference in RPO147 association by WT A19 and A19 with cysteine mutations. The strategy was to infect cells with vFS-A19i in the absence of IPTG as before but add cytosine arabinoside (AraC) to prevent viral DNA replication. Under these conditions, early genes such as the RNA polymerase gene will be expressed, but intermediate and late genes such as A19 and RAP94 genes will not. However, the wild-type and mutated A19 can be expressed from transfected plasmids under the control of an intermediate promoter even in the presence of AraC, because the intermediate transcription factors are early proteins. In addition to plasmids expressing the wild-type and mutated FS-A19, we also transfected a plasmid expressing FS-H7 as an affinity tag control in other cells. After purification with streptavidin-agarose, Western blotting showed that RPO 147 was associated with wild-type FS-A19 but not with either the control FS-H7 or FS-A19 with cysteine mutations (Fig. 7B, right). These results confirmed our conclusions that RAP94 is not required to mediate the association between A19 and RNA polymerase and that the putative zinc finger domain may be involved in this interaction.

Protein content and transcriptional activity of A19-deficient virus particles. Since A19 associates with RNA polymerase but is not required for postreplicative gene expression, we investigated whether A19 was needed for packaging or function of the early transcription complex. In the companion report (2), we showed that virus particles lacking A19 but containing DNA and the major virion proteins could be purified from cells infected with vFS-A19i in the absence of IPTG. When we probed Western blots prepared from $A19^+$ and $A19^-$ particles with the appropriate antibodies, we detected no differences in the relative amounts of RPO147, RAP94, and A7 and D6 transcription factors, suggesting that association with A19 is not required for packaging of the transcription complex (Fig. 8A).

Next, we compared the transcriptional activities of sucrose gradient-purified $A19^+$ and $A19^-$ virus particles. The two types of particles were isolated from equivalent gradient fractions, indicating that the difference in shape had little effect. For a control, we also purified $L3^+$ and $L3^-$ virions from cells infected with an L3-inducible virus, as the latter are defective in transcription (24). We confirmed the transcriptional activities of $A19^+$ and $L3^+$ virions (Fig. 8B). However, like $L3^-$ virus particles, $A19^-$ virus particles exhibited very low transcriptional activity (Fig. 8B).

DISCUSSION

In the accompanying report (2), we showed that the A19 protein is synthesized following DNA replication and is a minor component of the virion core. Further studies with a conditional lethal null mutant demonstrated that A19 is required for VACV morphogenesis. In the absence of A19, the assembly of VACV was altered

TABLE 2 Viral proteins associated with the A19 protein

VACV ORF	Protein or function	Normalized spectral counts		
		vFS-A19	vFS-A11	WR
A25L (84 kDa)	Nonspecific binding normalization	37	36	32
A19L (15 kDa[a])	FS-tagged protein	66	0	9
A11L (36 kDa)	FS-tagged protein	11	86	0
Transcription complex				
H4L (94 kDa)	RAP94	322	31	4
J6R (147 kDa)	RPO147	85	17	0
A24R (133 kDa)	RPO132	85	23	0
D1R (97 kDa)	Capping enzyme large subunit	31	17	2
A7L (82 kDa)	VETF large subunit	38	2	0
D6R (67 kDa)	VETF small subunit	11	0	0
D11L (72 kDa)	NPH I ATPase	15	0	0
Structural proteins				
A12L (21 kDa)	Core protein morphogenesis	70	10	0
A3L (73 kDa)	P4B core protein morphogenesis	46	5	11
E2L (86 kDa)	Virion protein morphogenesis	32	0.9	0.9

[a] This mass includes the FS tag.

prior to formation of infectious barrel-shaped particles, resulting in an accumulation of electron-dense, spherical, noninfectious particles lacking the D13 scaffold, of which some were wrapped with additional membrane and exited cells to become extracellular virus. This general phenotype is shared with several other VACV mutants with diverse roles, making it difficult to predict the function of A19. To gain insights, the amino acid sequence alignments of A19 homologs from each chordopoxvirus genus were compared. We noted two potentially interesting conserved features: a positively charged sequence that suggested a NLS or DNA/RNA binding domain and a pair of CXXC motifs that could represent a zinc finger or redox active cysteines. Site-directed mutagenesis demonstrated a requirement of the cysteines for A19 to complement the infectivity of the A19 null mutant. However, these mutations did not inactivate the VACV-specific redox system, leaving open the possibility of a role for the zinc finger domain. Zinc fingers are known to contribute to protein-protein interactions and to DNA binding (39). In contrast to the strong requirement for the conserved cysteines, mutation of the positively charged arginine residues to alanine reduced complementation by only 60%. Furthermore, although A19 was observed in the nucleus and in the cytoplasm, this distribution was unaffected by the mutations of the putative NLS. We do not know whether nuclear localization has special significance for A19.

To find clues to the role of A19, we affinity purified FS-A19 and analyzed the associated proteins by mass spectrometry. An important feature of this screen was the use of two controls: a virus that had the same affinity tag appended to a different protein and another virus in which there was no affinity tag. In this way, we could ascertain specificity for proteins associated with the A19 sequence. We were able to confirm by mass spectrometry the association of A19 with A12, previously found in a VACV genome-wide yeast two-hybrid analysis (20). The mass spectrometry analysis also detected A3, one of the most abundant core proteins, which like A12, also undergoes proteolytic processing by the I7 protease (7, 8, 15) and the E2 virion protein. Moreover, conditional lethal A12 and A3 mutants also exhibit defects at a late stage of morphogenesis (14, 15). However, using available antibodies for A3 and E2, we were unable to confirm their interaction with A19; A12 antibody was unavailable.

While the interaction of A19 with A12 and A3 was not surprising, as they are all core proteins involved in morphogenesis, interaction with the transcription complex was unexpected. The interaction was established, using mass spectrometry, by the detection of peptides corresponding to sequences within the two large subunits of RNA polymerase, RAP94, both subunits of the early transcription factor, NPH I, and the large subunit of the capping enzyme. Western blotting was used to confirm some of the mass spectrometry results and to extend the analysis. Western blotting with antibody to the 22-kDa subunit of RNA polymerase and the 147-kDa subunit suggested that the entire multisubunit RNA polymerase was affinity purified with A19 but that the small subunits were not detected by mass spectrometry. Indeed, most of the proteins detected by mass spectrometry in this study had masses of about 70 kDa or more (Table 2). RAP94 was also detected by Western blotting, but not the transcription factor subunits possibly because of low sensitivity of Western blotting with the available antibodies and an indirect association with A19. Since the components of the early transcription complex, including the RNA polymerase, RAP94, capping enzyme, NPH I, and early transcription factors, are associated through multiple interactions (22, 25, 40–42), it is difficult to determine which polypeptide interacts directly with A19. However, the available evidence points to the RNA polymerase for the following reasons. First, RNA polymerase associated with A19 when RAP94 was repressed, indicating that the latter protein does not mediate the interaction. Second, in the presence of AraC, intermediate and late proteins, including RAP94, the early transcription factor, and NPH I are not synthesized from the viral genome (43); yet when FS-A19 was selectively expressed from a transfected plasmid, RNA polymerase was pulled down. Therefore, A19 most likely interacts directly with the RNA polymerase, though interaction with the capping enzyme subunits, which also have early promoters, could not be excluded. In our current model, RAP94 is pulled down with A19, because

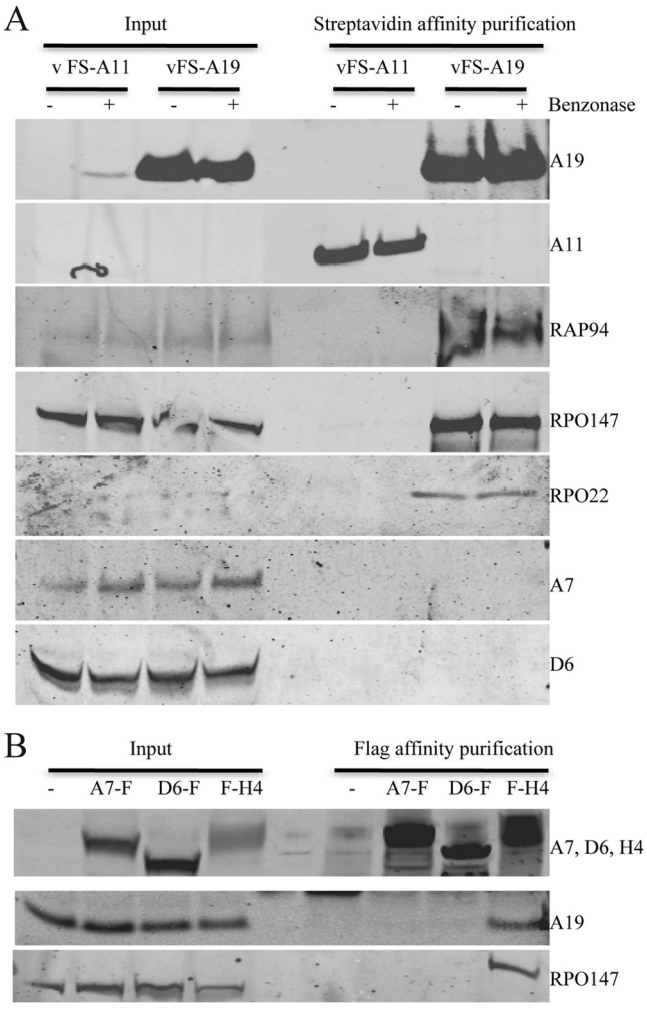

FIG 6 Western blots of A19-interacting proteins. (A) BS-C-1 cells were infected with vFS-A11 or vFS-A19 virus at 3 PFU/cell for 16 h. The cells were lysed in Triton X-100 for 30 min at 4°C and treated with Benzonase for an additional 30 min at room temperature. The soluble extract obtained after clarification by centrifugation (Input) was bound to streptavidin-agarose beads at 4°C for 16 h, washed, and eluted with lysis buffer containing D-biotin. Following SDS-PAGE, the proteins were transferred to a membrane and probed with antibodies to FLAG (A11 and A19) or to the other VACV proteins indicated on the right. The input contained very low concentrations of A11, RAP94, and A22 proteins, which were concentrated by the affinity purification. (B) Reverse affinity purification. BS-C-1 cells were infected with vHA-A19 (−), vA7-3XFlag/HA-A19 (A7-F), vD6-3XFlag/HA-A19 (D6-F), and v3XFlag-H4/HA-A19 (F-H4) for 16 h. Lysates were clarified and affinity purified by binding to FLAG M2 MAb conjugated to beads for 16 h at 4°C. The beads were washed, and bound proteins were eluted by boiling in lithium dodecyl sulfate loading buffer with reducing agent. Western blots were probed with anti-FLAG MAb to detect A7, D6, and H4 proteins, anti-HA MAb to detect A19, and antibody to RPO147. Note that H4 is the ORF encoding RAP94.

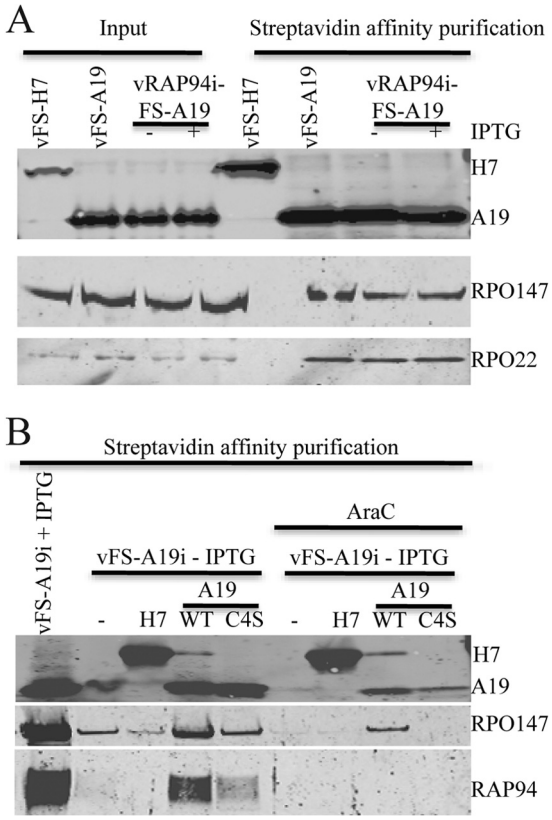

FIG 7 A19 interaction with RNA polymerase. (A) A19 interaction with RNA polymerase in the absence of RAP94. BS-C-1 cells were infected with vRAP94i-FS-A19 in the presence (+) and absence (−) of IPTG to regulate RAP94 expression and with negative and positive controls vFS-H7 and vFSA19 in the absence of IPTG, respectively. After 16 h, the cells were lysed, and the proteins were purified with streptavidin-agarose beads. Following SDS-PAGE, Western blotting was carried out with antibody to FLAG to detect H7 and A19 proteins and with rabbit polyclonal antibody to RPO147 and RPO 2. The left part of the blot shows the input lysate prior to affinity purification; the right part of the blot shows the affinity-purified proteins. (B) A19 interaction with RNA polymerase in the absence of other viral intermediate and late proteins. BS-C-1 cells were infected with vFS-A19i in the presence of IPTG as a control or without IPTG in the absence (left) or presence (right) of AraC and not transfected (−) or transfected with plasmids expressing FS-H7 (H7), wild-type FS-A19 (WT), and FS-A19 with serine substitutions of the four conserved cysteines (C4S). The proteins were affinity purified and analyzed by Western blotting as described above for panel A. FLAG MAb was used to detect H7 and A19 proteins, and rabbit polyclonal antibodies were used to detect RPO147 and RAP94 proteins.

the latter interacts with RNA polymerase (30, 38); NPH I (42) and A7 and D6 (25) are pulled down because of their association with RAP94. At this time, we are unable to predict the interacting subunit(s) of the RNA polymerase. The putative zinc finger domain is a possible interaction site on A19, since mutation of the conserved cysteines reduced the interaction of A19 with the transcription complex.

Repression of RAP94 results in the failure to package RNA polymerase, capping enzyme, and NPH I, but not VETF, leading to a model in which VETF binds to early promoters and attracts the transcription enzyme complex through RAP94 (22, 25). However, repression of A19 did not impair the incorporation of the transcription complex or the A3 core protein (2), into virus particles. Nevertheless, A19$^-$ virus particles were defective in transcription. In this respect, the phenotypes of A19$^-$, L3$^-$ (24), and A3$^-$ (14) virus particles are similar. However, although repression of A3, like A19, also results in dense, spherical particles, repression of L3 does not result in an obvious arrest in morphogenesis, and interacting proteins have not been identified.

The relationship between the block in morphogenesis, RNA polymerase association, and defect in transcription is difficult to

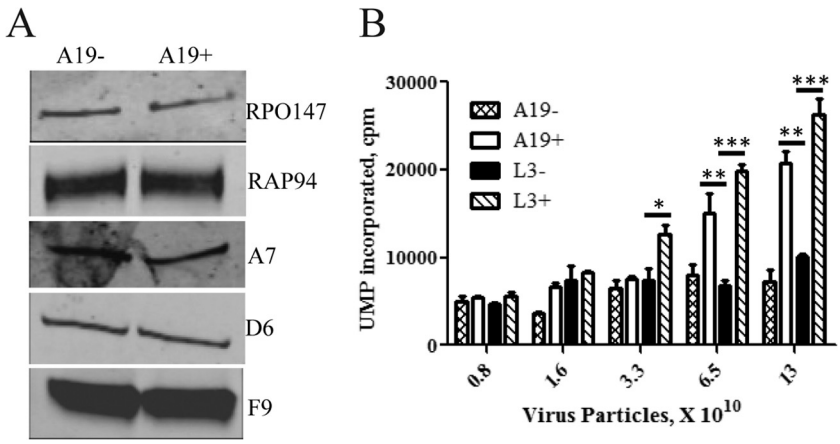

FIG 8 Protein composition and transcriptional activity of purified virus particles. (A) Protein composition. Virus particles were purified by sucrose density gradient centrifugation from BS-C-1 cells that had been infected with vFS-A19i virus in the absence of IPTG (A19−) or presence of IPTG (A19+). Proteins from equivalent amounts of A19-deficient and A19-containing virus particles, determined by optical density, were resolved by SDS-PAGE, transferred to a nitrocellulose membrane, and probed with rabbit polyclonal antibodies to the proteins indicated on the right. (B) Transcriptional activity. Virus particles were purified by sucrose gradient sedimentation from cells infected with vFS-A19i or vL3i in the presence of IPTG (+) or absence of IPTG (−). RNA synthesis was measured by incorporation of [α-^{32}P]UMP in reaction mixtures containing the indicated numbers of virus particles determined from optical density. The results are presented as UMP incorporated. Error bars are shown. Statistical significance was determined by one-way ANOVA as follows: *, $P > 0.05$; **, $P < 0.05$; ***, $P < 0.001$.

explain. A L3 null mutant, which is defective in transcription, makes normal-looking mature virions (24), and a RAP94 null mutant, which does not package RNA polymerase, also makes normal-looking mature virions (22). Therefore, a transcription capability of virions is not necessary for morphogenesis. This could suggest that the A19 requirement for morphogenesis is independent of its interaction with RNA polymerase. However, early transcription factor null mutants have a defect in morphogenesis (12, 13). Consequently, we cannot rule out the possibility that RNA polymerase unassociated with A19 has a dominant-negative effect, even though absence of RNA polymerase does not interfere with morphogenesis. Furthermore, we cannot tell whether the defect in transcription is secondary to the block in morphogenesis or whether A19 is more directly involved in transcription due to its association with RNA polymerase. In view of the propensity for viruses to maximize use of their coding capacity, we would not be surprised if A19 turns out to have multiple functions.

Approximately 50 proteins have been detected in VACV cores (1), but there is little information regarding their protein interactions and location within the virion. Exceptions are the early transcription complex, comprising about 15 polypeptides, including RNA polymerase, and the so-called seven-protein complex (44). The finding that A19 stably associates with the RNA polymerase and the two core proteins A3 and A12 provides another step toward the goal of defining the virion interactome.

ACKNOWLEDGMENTS

We thank Catherine Cotter of the Laboratory of Viral Diseases, National Institute of Allergy and Infectious Diseases (NIAID), for help preparing cell cultures and Sundar Ganesan and Juraj Kabat from the NIAID biological imaging facility for help with confocal analysis.

This research was supported by intramural funds of the National Institute of Allergy and Infectious Diseases, National Institutes of Health.

REFERENCES

1. **Condit RC, Moussatche N, Traktman P.** 2006. In a nutshell: structure and assembly of the vaccinia virion. Adv. Virus Res. **66:**31–124.
2. **Satheshkumar PS, Weisberg AS, Moss B.** 2013. Vaccinia virus A19 protein participates in the transformation of spherical immature particles to barrel-shaped infectious virions. J. Virol. **87:**10700–10709.
3. **Cassetti MC, Merchlinsky M, Wolffe EJ, Weisberg AS, Moss B.** 1998. DNA packaging mutant: repression of the vaccinia virus A32 gene results in noninfectious, DNA-deficient, spherical, enveloped particles. J. Virol. **72:**5769–5780.
4. **Grubisha O, Traktman P.** 2003. Genetic analysis of the vaccinia virus I6 telomere-binding protein uncovers a key role in genome encapsidation. J. Virol. **77:**10929–10942.
5. **Garcia AD, Moss B.** 2001. Repression of vaccinia virus Holliday junction resolvase inhibits processing of viral DNA into unit-length genomes. J. Virol. **75:**6460–6471.
6. **Senkevich TG, Koonin EV, Moss B.** 2009. Predicted poxvirus FEN1-like nuclease required for homologous recombination, double-strand break repair and full-size genome formation. Proc. Natl. Acad. Sci. U. S. A. **106:**17921–17926.
7. **Ansarah-Sobrinho C, Moss B.** 2004. Role of the I7 protein in proteolytic processing of vaccinia virus membrane and core components. J. Virol. **78:**6335–6343.
8. **Byrd CM, Hruby DE.** 2005. A conditional-lethal vaccinia virus mutant demonstrates that the I7L gene product is required for virion morphogenesis. Virol. J. **2:**4. doi:10.1186/1743-422X-2-4.
9. **Moerdyk MJ, Byrd CM, Hruby DE.** 2006. Analysis of vaccinia virus temperature-sensitive I7L mutants reveals two potential functional domains. Virol. J. **3:**64. doi:10.1186/1743-422X-3-64.
10. **Ansarah-Sobrinho C, Moss B.** 2004. Vaccinia virus G1 protein, a predicted metalloprotease, is essential for morphogenesis of infectious virions but not for cleavage of major core proteins. J. Virol. **78:**6855–6863.
11. **Hedengren-Olcott M, Byrd CM, Watson J, Hruby DE.** 2004. The vaccinia virus G1L putative metalloproteinase is essential for viral replication in vivo. J. Virol. **78:**9947–9953.
12. **Hu X, Wolffe EJ, Weisberg AS, Carroll LJ, Moss B.** 1998. Repression of the A8L gene, encoding the early transcription factor 82-kilodalton subunit, inhibits morphogenesis of vaccinia virions. J. Virol. **72:**104–112.
13. **Hu X, Carroll LJ, Wolffe EJ, Moss B.** 1996. *De novo* synthesis of the early transcription factor 70-kDa subunit is required for morphogenesis of vaccinia virions. J. Virol. **70:**7669–7677.
14. **Kato SEM, Strahl AL, Moussatche N, Condit RC.** 2004. Temperature-sensitive mutants in the vaccinia virus 4b virion structural protein assemble malformed, transcriptionally inactive intracellular mature virions. Virology **330:**127–146.
15. **Yang SJ, Hruby DE.** 2007. Vaccinia virus A12L protein and its AG/A

proteolysis play an important role in viral morphogenic transition. Virol. J. **4:**73. doi:10.1186/1743-422X-4-73.
16. **Kusakabe T, Hine AV, Hyberts SG, Richardson CC.** 1999. The Cys4 zinc finger of bacteriophage T7 primase in sequence-specific single-stranded DNA recognition. Proc. Natl. Acad. Sci. U. S. A. **96:**4295–4300.
17. **Frand AR, Cuozzo JW, Kaiser CA.** 2000. Pathways for protein disulphide bond formation. Trends Cell Biol. **10:**203–210.
18. **Lange A, Mills RE, Lange CJ, Stewart M, Devine SE, Corbett AH.** 2007. Classical nuclear localization signals: definition, function, and interaction with importin alpha. J. Biol. Chem. **282:**5101–5105.
19. **LaCasse EC, Lefebvre YA.** 1995. Nuclear localization signals overlap DNA- or RNA-binding domains in nucleic acid-binding proteins. Nucleic Acids Res. **23:**1647–1656.
20. **McCraith S, Holtzman T, Moss B, Fields S.** 2000. Genome-wide analysis of vaccinia virus protein-protein interactions. Proc. Natl. Acad. Sci. U. S. A. **97:**4879–4884.
21. **Alexander WA, Moss B, Fuerst TR.** 1992. Regulated expression of foreign genes in vaccinia virus under the control of bacteriophage T7 RNA polymerase and the *Escherichia coli lac* repressor. J. Virol. **66:**2934–2942.
22. **Zhang Y, Ahn B-Y, Moss B.** 1994. Targeting of a multicomponent transcription apparatus into assembling vaccinia virus particles requires RAP94, an RNA polymerase-associated protein. J. Virol. **68:**1360–1370.
23. **Senkevich TG, Weisberg A, Moss B.** 2000. Vaccinia virus E10R protein is associated with the membranes of intracellular mature virions and has a role in morphogenesis. Virology **278:**244–252.
24. **Resch W, Moss B.** 2005. The conserved poxvirus L3 virion protein is required for transcription of vaccinia virus early genes. J. Virol. **79:**14719–14729.
25. **Yang Z, Moss B.** 2009. Interaction of the vaccinia virus RNA polymerase-associated 94-kilodalton protein with the early transcription factor. J. Virol. **83:**12018–12026.
26. **Wolffe EJ, Vijaya S, Moss B.** 1995. A myristylated membrane protein encoded by the vaccinia virus L1R open reading frame is the target of potent neutralizing monoclonal antibodies. Virology **211:**53–63.
27. **Lustig S, Fogg C, Whitbeck JC, Eisenberg RJ, Cohen GH, Moss B.** 2005. Combinations of polyclonal or monoclonal antibodies to proteins of the outer membranes of the two infectious forms of vaccinia virus protect mice against a lethal respiratory challenge. J. Virol. **79:**13454–13462.
28. **Gershon PD, Moss B.** 1990. Early transcription factor subunits are encoded by vaccinia virus late genes. Proc. Natl. Acad. Sci. U. S. A. **87:**4401–4405.
29. **Resch W, Weisberg AS, Moss B.** 2005. Vaccinia virus nonstructural protein encoded by the A11R gene is required for formation of the virion membrane. J. Virol. **79:**6598–6609.
30. **Ahn B-Y, Moss B.** 1992. RNA polymerase-associated transcription specificity factor encoded by vaccinia virus. Proc. Natl. Acad. Sci. U. S. A. **89:**3536–3540.
31. **Brown E, Senkevich TG, Moss B.** 2006. Vaccinia virus F9 virion membrane protein is required for entry but not virus assembly, in contrast to the related L1 protein. J. Virol. **80:**9455–9464.
32. **Thompson JD, Higgins DG, Gibson TJ.** 1994. CLUSTAL W: improving the sensitivity of progressive multiple sequence alignment through sequence weighting, position-specific gap penalties and weight matrix choice. Nucleic Acids Res. **22:**4673–4680.
33. **Senkevich TG, White CL, Koonin EV, Moss B.** 2002. Complete pathway for protein disulfide bond formation encoded by poxviruses. Proc. Natl. Acad. Sci. U. S. A. **99:**6667–6672.
34. **Katsafanas GC, Moss B.** 2007. Colocalization of transcription and translation within cytoplasmic poxvirus factories coordinates viral expression and subjugates host functions. Cell Host Microbe **2:**221–228.
35. **Yuwen H, Cox JH, Yewdell JW, Bennink JR, Moss B.** 1993. Nuclear localization of a double-stranded RNA-binding protein encoded by the vaccinia virus E3l gene. Virology **195:**732–744.
36. **Senkevich TG, Koonin EV, Moss B.** 2011. Vaccinia virus F16 protein, a predicted catalytically inactive member of the prokaryotic serine recombinase superfamily, is targeted to nucleoli. Virology **417:**334–342.
37. **Moss B.** 2012. Poxvirus cell entry: how many proteins does it take? Viruses **4:**688–707.
38. **Kane EM, Shuman S.** 1992. Temperature-sensitive mutations in the vaccinia virus H4 gene encoding a component of the virion RNA polymerase. J. Virol. **66:**5752–5762.
39. **Gamsjaeger R, Liew CK, Loughlin FE, Crossley M, Mackay JP.** 2007. Sticky fingers: zinc-fingers as protein-recognition motifs. Trends Biochem. Sci. **32:**63–70.
40. **Broyles SS, Moss B.** 1987. Sedimentation of an RNA polymerase complex from vaccinia virus that specifically initiates and terminates transcription. Mol. Cell. Biol. **7:**7–14.
41. **Katsafanas GC, Moss B.** 1999. Histidine codons appended to the gene encoding the RPO22 subunit of vaccinia virus RNA polymerase facilitate the isolation and purification of functional enzyme and associated proteins from virus-infected cells. Virology **258:**469–479.
42. **Mohamed MR, Niles EG.** 2000. Interaction between nucleoside triphosphate phosphohydrolase I and the H4L subunit of the viral RNA polymerase is required for vaccinia virus early gene transcript release. J. Biol. Chem. **275:**25798–25804.
43. **Yang Z, Bruno DP, Martens CA, Porcella SF, Moss B.** 2010. Simultaneous high-resolution analysis of vaccinia virus and host cell transcriptomes by deep RNA sequencing. Proc. Natl. Acad. Sci. U. S. A. **107:**11513–11518.
44. **Szajner P, Jaffe H, Weisberg AS, Moss B.** 2004. A complex of seven vaccinia virus proteins conserved in all chordopoxviruses is required for the association of membranes and viroplasm to form immature virions. Virology **330:**447–459.